JACS Au
AN OPEN ACCESS JOURNAL OF THE AMERICAN CHEMICAL SOCIETY

pubs.acs.org/jacsau Article

Nature of Catalytic Behavior of Cobalt Oxides for CO_2 Hydrogenation

Kailang Li, Xianghong Li, Lulu Li, Xin Chang, Shican Wu, Chengsheng Yang, Xiwen Song, Zhi-Jian Zhao,* and Jinlong Gong*

Cite This: *JACS Au* 2023, 3, 508−515 Read Online

ACCESS | Metrics & More | Article Recommendations | Supporting Information

ABSTRACT: Cobalt oxide (CoO_x) catalysts are widely applied in CO_2 hydrogenation but suffer from structural evolution during the reaction. This paper describes the complicated structure−performance relationship under reaction conditions. An iterative approach was employed to simulate the reduction process with the help of neural network potential-accelerated molecular dynamics. Based on the reduced models of catalysts, a combined theoretical and experimental study has discovered that CoO(111) provides active sites to break C−O bonds for CH_4 production. The analysis of the reaction mechanism indicated that the C−O bond scission of $^*CH_2O$ species plays a key role in producing CH_4. The nature of dissociating C−O bonds is attributed to the stabilization of *O atoms after C−O bond cleavage and the weakening of C−O bond strength by surface-transferred electrons. This work may offer a paradigm to explore the origin of performance over metal oxides in heterogeneous catalysis.

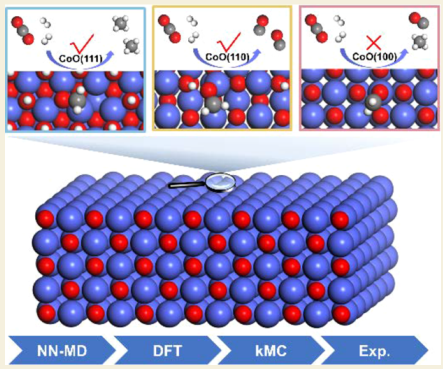

KEYWORDS: *CO_2 hydrogenation, structure−performance relationship, CoO catalysts, density functional theory, multiscale simulation*

■ INTRODUCTION

The efficient utilization of greenhouse gas CO_2 has always been of considerable attraction. CO_2 hydrogenation is a mature technology, which not only can convert CO_2 into high value-added chemicals but also mitigate the greenhouse effect by the consumption of CO_2.[1−3] Co-based CO_2 hydrogenation catalysts are widely applied in methanation,[4] methanol production,[5] and C−C coupling reactions, i.e., the synthesis of long-chain alkanes[6] and higher alcohols.[7,8] However, the key factors that affect catalytic performance are still controversial, which are possibly related to, for instance, size dependence,[9] metal−support interaction,[10] crystal facet dependence,[11,12] surface segregation,[13] and coverage effect.[14]

In particular, the structures of Co-based oxide catalysts are complex with variable valence states under reaction conditions.[15] Co_3O_4 is a typical representative that exhibits structure sensitivity during CO_2 hydrogenation.[16,17] To be more specific, variations in catalyst morphology lead to significant differences in product distribution. Co_3O_4 nanoparticles display high selectivity for CH_4, while Co_3O_4 nanorods tend to produce CO. In the meantime, Co_3O_4 is not stable during the reaction. Phase transformation induced by H_2 occurs, where Co_3O_4 is reduced to CoO or even metallic Co. As a result, CoO is believed to be the main active phase during CO_2 hydrogenation.[18] The complexity of dynamically structural evolution in bulk and surface makes it challenging to interpret the origin of performance over cobalt oxides (CoO_x).

Limited by current *in situ* characterization techniques, it is hard to accurately identify the complex feature sites and perceive the evolution of feature structures. Although density functional theory (DFT) calculations can provide atomic-scale insights into the rational design of catalysts, the expensive computational cost prevents realizing large-scale and long-term simulations, leading to a large gap between simulated models and real catalytic systems. Hopefully, machine learning techniques[19,20] enable breaking through the dilemma and surmount the spatial and temporal limitations of DFT by accelerating the time-consuming simulation with an affordable computational cost, pointing out a promising route to describe the dynamic catalyst behavior at the atomic level during the reaction.[21,22]

Here, neural network potential-based molecular dynamics (NN-MD) simulations were carried out to probe the dynamically structural evolution from Co_3O_4 to CoO according to experimental reduction conditions. With the application of DFT calculations, kinetic Monte Carlo (kMC) simulations, and experimental studies, the correlation between structure and selectivity was established at the atomic level. We

Received: November 17, 2022
Revised: January 1, 2023
Accepted: January 17, 2023
Published: February 1, 2023

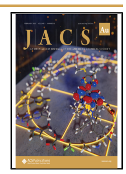

revealed the nature of C−O bond dissociation on feature structures and provided a clear perspective on the reaction mechanism of CoO verified by our experiments. This work can offer a theoretical guidance for rational design of CoO_x catalysts in CO_2 hydrogenation by a practical multiscale research method for establishing the structure−performance relationship of metal oxides in heterogeneous catalysis.

RESULTS AND DISCUSSION

Structural Evolution

In order to understand the dynamically structural evolution of Co_3O_4 under the reaction condition, NN-MD simulations were employed to simulate the reduction process of the precursor, i.e., Co_3O_4. The commonly exposed crystalline surfaces of experimentally synthesized nanostructure catalysts, i.e., Co_3O_4(100), Co_3O_4(110), and Co_3O_4(111),[18] were chosen as the model surfaces prior to the reduction with a scale of about 1000 atoms in one unit cell. The reduction process was simulated by two iterative steps, which are surface reduction and reconstruction (Figure 1a).[23] To begin the reduction process, O vacancy formation free energies (G_{O_v}) of surface O atoms under experimental reduction conditions were calculated, and the ones with negative values were removed to mimic surface reduction reactions. Afterward, the partially reduced surface reached equilibrium by 1.5 ns NN-MD simulations with a canonical ensemble (NVT), during which some subsurface O atoms might diffuse to the surface. Then, another round of reduction-reconstruction simulation started, until G_{O_v} values of all surface O atoms are greater than 0 eV, implying that the surface cannot be further reduced thermodynamically (Scheme S1 and Figures S1−S9). The feature structures after reduction were consequently confirmed via NN-MD.

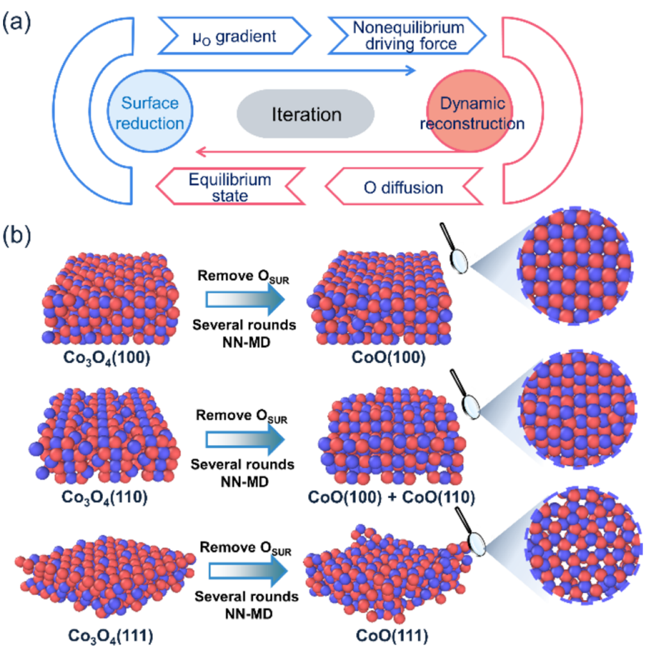

Figure 1. (a) Principle of surface reaction-reconstruction to simulate the reduction process of Co_3O_4. μ_O represents the chemical potential of O atoms. (b) NN-MD simulations of the reduction process on the Co_3O_4 model. Color code: blue-Co; red-O.

It is gratifying that the obtained reduced surface model is consistent with the experimental observations that the CoO phase is the main active phase of CoO_x catalysts in CO_2 hydrogenation.[24] From the simulated surface structures where the ratio of Co and O atoms is about 1:1.(Figure 1b), the regular CoO(100) facet is observed after the reduction of Co_3O_4(100). The reduced Co_3O_4(110) mainly exposes CoO(110)- and CoO(100)-like structures, accompanied by few defective sites, like grain boundaries and oxygen vacancies. The CoO(111) facet with a small portion of oxygen vacancies and clusters is obtained after the reduction of Co_3O_4(111). So far, three feature structures after reduction, CoO(100), CoO(110), and CoO(111), have been obtained via our iterative reduction simulations.

Structure−Performance Relationship

On the basis of these surface structures, small slab models were selected for accurate DFT calculations. Over the oxide catalysts, hydroxyl groups (OH) and oxygen vacancies (O_v) may form, induced by the H_2 atmosphere. Hence, thermodynamic phase diagrams were calculated with consideration of the possible presence of OH and O_v, and the stable structures were confirmed under the reaction condition (T = 573 K and p_{H2} = 0.2 atm), which are clean CoO(100), CoO(110) with 1/4 ML OH, and CoO(111) with 7/9 ML OH (Figures S10 and S11).

We further explored the structure−performance relationship of CoO and compared it with the metallic Co that may appear after the reaction.[16,25] CO_2 activation, as the initial step of CO_2 hydrogenation, has an essential impact on subsequent reactions. After adsorption, the CO_2 molecule tends to be bent as it acquires electrons from the surface. Straightforwardly, the changes in configurations can visualize the activation ability of different structures. Among them, the most obvious variation of CO_2 configuration occurs on CoO(111). The C═O bond length increases from 1.18 to 1.39 Å and ∠OCO decreases from 180 to 122°, indicating that CO_2 could be easily activated on CoO(111) (Figure 2a). Analyzed by charge transfer, the CO_2 molecule adsorbed on CoO(111) acquires the most electrons (1.11 e) (Figure S16). The transferred electrons fill in the antibonding orbitals of CO_2, which can activate the C═O bond and promote the CO_2 molecule to be adsorbed in the form of bending rather than linear.[26]

The reaction mechanisms of CO_2 hydrogenation are mainly divided into the formate pathway, carboxyl pathway, and direct C−O dissociation pathway,[27] while it is generally accepted that direct dissociation of the C−O bond is very difficult without the involvement of H.[28,29] In the first place, the carboxyl pathway (RWGS reaction + CO hydrogenation) was taken into account, because CO is the reaction product and key reaction intermediate for cobalt oxides,[15] and its further hydrogenation is believed as an efficient route that is responsible for the formation of deep reduction products.[30] Here, we started with CO hydrogenation to *CHO, as well as its competition step CO desorption, to explore deep reduction capacity (Figure 2b). Surprisingly, our calculated barriers of further hydrogenation are always higher than corresponding CO desorption barriers over all the cobalt oxide module surfaces. Therefore, the CO intermediate is hard to be reduced, which prefers desorption as a product.

CH_4 is another main product of cobalt oxides in CO_2 hydrogenation besides CO.[18,25] As a deep reduction product,

https://doi.org/10.1021/jacsau.2c00632
JACS Au 2023, 3, 508−515

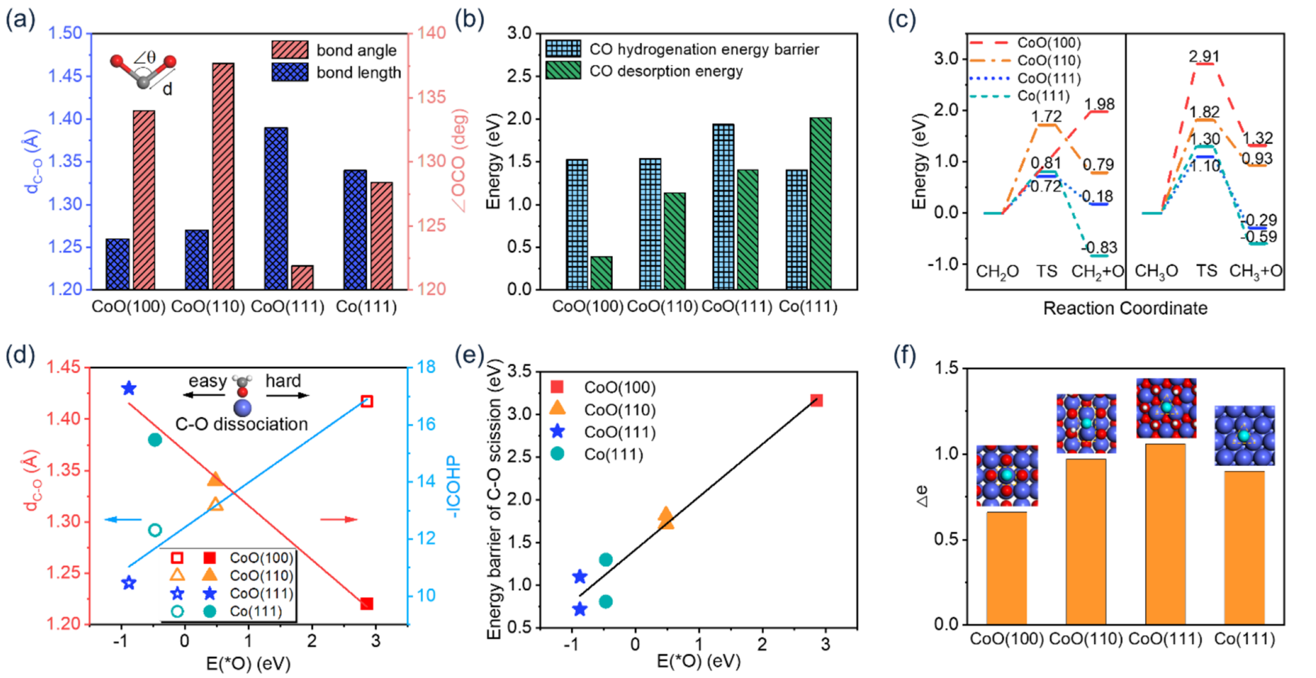

Figure 2. (a) Bond lengths and bond angles of adsorbed $*CO_2$ on different surfaces. (b) Energy profile for CO hydrogenation and desorption on different surfaces. (c) Energy profile for C−O bond dissociation on different surfaces. (d) Red: The relationship between E(*O) and the C−O bond length; blue: the relationship between E(*O) and -ICOHP of the C−O bond. (e) Relationship between E(*O) and C−O bond dissociation. (f) Electron transfer of adsorbed *O on different surfaces.

CH_4 tends to be generated via the formate pathway as analyzed above. The C−O bond dissociation of $*CH_xO$ is critical to produce CH_4 under the formate pathway, suggesting that $*CH_xO$ intermediates serve as key species to determine CH_4 selectivity.[15,31−33] Since *CHO needs to cross the relatively high barrier to be dissociated (Figure S39), $*CH_2O$ and $*CH_3O$ species were selected as possible precursors for the C−O bond scission.[30] As shown in Figure 2c, for $*CH_2O$ and $*CH_3O$ species adsorbed on CoO(100) and CoO(110), the reaction is highly endothermic, which is thermodynamically unfavorable for C−O dissociation. In consequence, CoO(100) and CoO(110) need to overcome high barriers to break the C−O bond. On the contrary, CoO(111) is easy to dissociate the C−O bond with low barriers, which are even lower than metallic Co, effectively facilitating CH_4 production.

The C−O bond cleavage is usually related to the C−O bond length, the longer C−O bond length is more prone to break the C−O bond.[34] Interestingly, the adsorption energies of *O atoms (E(*O)) have a good linear relation with the C−O bond length (Figure 2d), implying that E(*O) may be used to reveal the nature of C−O bond scission. To further quantify the chemical bond strength, we calculated the integrated crystal orbital Hamilton population (ICOHP) of the C−O bond, where the smaller value of -ICOHP means the weaker C−O bond strength. Apparently, the stronger the *O atom is adsorbed on the surface, the smaller the -ICOHP is, indicating easier breaking the C−O bond and thereby promoting the production of CH_4. Hence, E(*O) can be a simple descriptor to measure C−O bond scission (Figure 2e).

We further explored essential factors that may lead to the difference in E(*O). The phenomenon can be explained by the analysis of geometric structures (Figure 2f). CoO(111) and Co(111) provide three-fold hollow sites to efficiently stabilize *O atoms after dissociation of $*CH_xO$ intermediates. However, *O on CoO(110) and CoO(100) can only be adsorbed on top and bridge sites, resulting in the instability of *O atoms with high barriers for breaking the C−O bond, and thereby inhibiting the formation of CH_4. In addition, the electron transfer is equally vital. Compared with other surfaces, the *O atom on CoO(111) acquires more electrons (1.06 e) from the surface. The transferred electrons can fill in the antibonding orbitals of the C−O bond of $*CH_xO$ to weaken the C−O bond strength, promoting to break C−O bonds. Therefore, the nature of C−O bond dissociation is attributed to the stabilization of *O atoms after C−O bond cleavage, and the weakening of C−O bond strength via surface-transferred electrons.

Kinetic Investigation

To gain a comprehensive insight into the catalytic mechanism of CoO in CO_2 hydrogenation, the whole reaction networks were constructed by the combination of DFT calculations and kMC simulations with CoO(111) as a representative that exhibits wonderful capacities of CO_2 activation and C−O bond cleavage. As it is hard to break C−O bonds directly without the assistance of H,[28,29] the formate pathway and carboxyl pathway that involves H to assist in dissociating C−O bonds are considered as dominant reaction routes. The reaction network involves 21 different intermediates and 46 elementary steps. The relevant reaction energies and barriers, along with lateral interactions of coadsorption species, are listed in Tables S1 and S2.

As shown in Figure 3a,b, the CO_2 hydrogenation reaction is dominated by the production of CH_4 through the formate pathway, because the event frequency of *HCOO formation is between 2 and 3 orders of magnitude greater than that of *COOH production. After hydrogenation and dissociation of *HCOO, $*CH_2O$ is favorable to be formed without any high barrier to overcome. The formation of CH_4 mainly relies on the C−O bond dissociation of $*CH_2O$ and $*CH_3O$. The

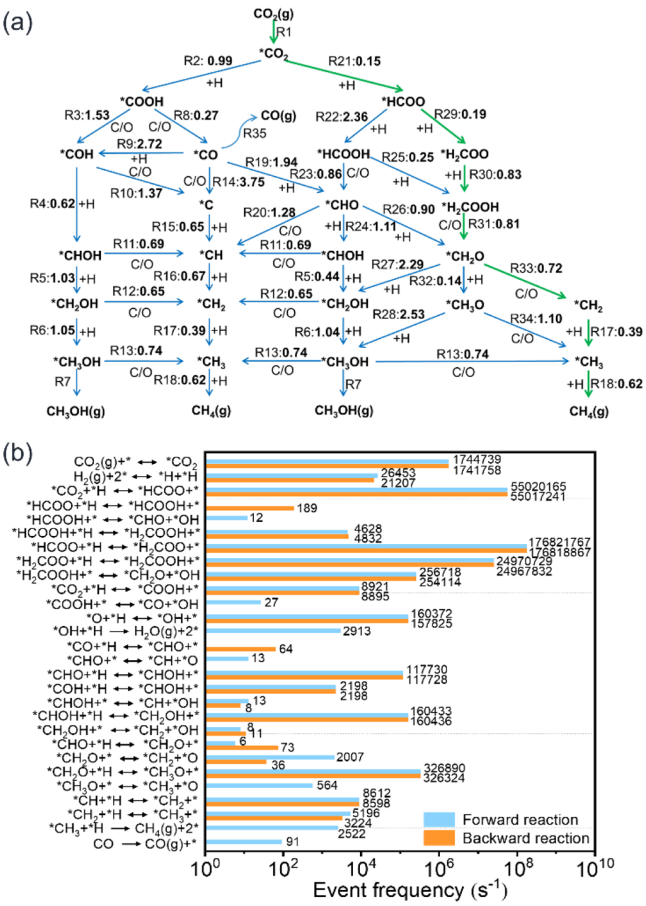

Figure 3. (a) Reaction networks of CoO(111) for CO_2 hydrogenation toward CO, CH_4, and CH_3OH based on DFT calculations. The values are barriers of hydrogenation and C−O dissociation. All values are in eV with ZPE correlation. The most favorable pathway toward CH_4 is highlighted with green bold arrows. (b) Event frequency for elementary steps on CoO(111) based on kMC simulations in CO_2 hydrogenation.

frequency of breaking the C−O bond of $*CH_2O$ is almost 4 times higher than that of $*CH_3O$, implying that the task on dissociating C−O bonds is mainly completed via $*CH_2O$ (R33, E_{act_fwd} = 0.72 eV), rather than $*CH_3O$ (R34, E_{act_fwd} = 1.10 eV). Thus, the C−O bond scission of $*CH_2O$ becomes the critical step to determine the CH_4 selectivity. In addition, as the other product, the main bottleneck for CO to be deeply reduced is that the desorption of *CO (R35, E_{act_fwd} = 1.51 eV) is more favorable than further hydrogenation or cleavage of *CO to generate *C (R14, E_{act_fwd} = 3.75 eV), *CHO (R19, E_{act_fwd} = 1.94 eV) or *COH (R9, E_{act_fwd} = 2.72 eV), suggesting that CO tends to be the product, which is consistent with the above analysis.

It is also worth noting that the removal of surface O species (*O and *OH) to form $H_2O_{(g)}$ plays a crucial role in the overall reaction rate. The process of *O hydrogenation to form *OH occurs frequently, but only a small portion of *OH on the surface can be further hydrogenated to produce H_2O (E_{act_fwd} = 1.56 eV). Hence, a high coverage of *OH is shown on the surface when the reaction reaches equilibrium (Table 1). The analysis of degree of rate control[35] indicates that *OH hydrogenation to H_2O controls the rate of the whole reaction (X_{RC} = 0.825), which is the rate-determining step (Table S3).

Table 1. Surface Species Coverage for the Reaction Equilibrium

species	θ (ML)[a]	species	θ (ML)[a]
$*CO_2$	31/3200	$*H_2COOH$	95/3200
*H	92/3200	$*CH_3O$	2/3200
*OH	2328/3200	*CH	4/3200
*HCOO	217/3200	$*CH_2$	10/3200
$*H_2COO$	2/3200	$*CH_3$	14/3200

[a]θ is the coverage of surface species; ML represents the monolayer.

Experimental Verification

To verify the structure−performance relationship of CoO catalysts in CO_2 hydrogenation, we synthesized CoO catalysts with relevant feature structures, matched with theoretical calculation models. Foremost, we prepared Co_3O_4 samples as the precursors via a hydrothermal method, where nanoparticles expose {111} + {001} facets and nanorods are enclosed with {110} + {001} facets.[18] Moreover, {111} and {110} facets take up most of the surface of nanoparticles and nanorods, respectively (Figure S31).[36] Though the treatment of H_2 at 573 K, the samples display CoO diffraction peaks from X-ray diffraction characterization (Figures S33 and S34). In addition, Co $2p_{3/2}$ peaks tested by X-ray photoelectron spectroscopy (XPS) shift from about 779.4 to 780.1 eV. Both of them indicate that Co_3O_4 is reduced to CoO (Figure S35).[37−39] After reduction, CoO catalysts retain nanoparticle and nanorod morphology, while preferential facets are altered. Co_3O_4(111) is transformed into CoO(111), and Co_3O_4(110) is converted to CoO(110) (Figure S32), which is consistent with the structural evolution from Co_3O_4 to CoO via NN-MD simulations.

Afterward, CoO catalysts were tested under the reaction condition (p = 1 atm, T = 573 K and CO_2/H_2 = 1:3) (Figure 4a). Reaction activity and product distribution change

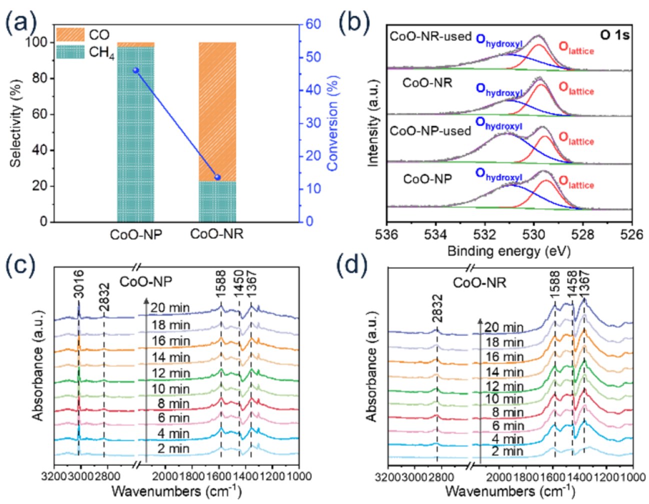

Figure 4. Experimental results of the synthesis catalysts. (a) Catalytic performance of CoO-NP and CoO-NR catalysts. Reaction conditions: p = 1 atm, T = 573 K, 0.15 g catalyst, CO_2/H_2 = 1:3. (b) O 1s XPS spectra of CoO-NP, CoO-NP-used, CoO-NR, and CoO-NR-used. In situ DRIFTS spectra of (c) CoO-NP and (d) CoO-NR. Reaction conditions: p = 1 atm, T = 573 K, CO_2/H_2 = 1:3. CoO-NP and CoO-NR represent CoO nanoparticles and nanorods after the reduction of Co_3O_4 by H_2; CoO-NP-used and CoO-NR-used represent CoO nanoparticles and nanorods after the CO_2 hydrogenation reaction.

https://doi.org/10.1021/jacsau.2c00632
JACS Au 2023, 3, 508−515

considerably as the morphology of CoO transforms. Upon converting nanoparticles to nanorods, CH_4 selectivity decreases from 98 to 23% and CO selectivity increases from 2 to 77%. Meanwhile, CO_2 conversion decreases from 46 to 13%. Apparently, CoO nanoparticles are more prone to catalyze the methanation reaction, possessing a stronger capacity to promote C−O bond cleavage with a higher reaction activity. Nevertheless, methanation on CoO nanorods is significantly inhibited. As a consequence, CO is the main product.

Notably, compared with CoO nanorods, a high fraction of hydroxyl O occurs on CoO nanoparticles after the reaction, where the binding energy of O 1s on about 529.5 and 531.5 eV is assigned to lattice O and hydroxyl O on surfaces (Figure 4b).[37,44−46] It suggests that the removal of hydroxyl O over CoO(111) exposed on nanoparticles is hard and has a key impact on the overall reaction rate, in agreement with kMC simulations.

To demonstrate the accuracy of our proposed reaction mechanism, in situ DRIFTS was employed to observe surface intermediates (Figure 4c,d). The peaks at 2832, 1588, and 1367 cm^{-1} are assigned to stretching vibrations of the C−H bond, stretching, and bending vibrations of OCO, respectively, indicating the existence of *HCOO species.[40−42] In addition, compared with the weak peak at 1450 cm^{-1} over CoO nanoparticles, there is an obvious peak at 1458 cm^{-1} over CoO nanorods. They might correspond to the vibrational mode of $*CH_x$ in $*CH_xO$ species,[43] since the similar peaks are obtained by DFT calculations, which are related to the bending vibration of $*CH_2$ in $*CH_2O$ on CoO(111) (1431 cm^{-1}) and CoO(110) (1440 cm^{-1}). The phenomenon indicates the accumulation of $*CH_xO$ species on CoO nanorods (CoO(110)), due to the poor capability for C−O bond scission. Inversely, it is easy for CoO nanoparticles (CoO(111)) to break C−O bonds, leading to rapid consumption of $*CH_xO$. As a result, the signal peak of CH_4 on 3016 cm^{-1} can be clearly observed.

CONCLUSIONS

In summary, this paper presents a multiscale calculation method to deal with a complex structure−performance relationship over CoO_x catalysts. Through employing the surface reduction-reconstruction approach to simulate the reduction process of cobalt oxides via NN-MD, three theoretical models have been obtained with the application of the surface phase diagram, which are clean CoO(100), CoO(110) with 1/4 ML OH, and CoO(111) with 7/9 ML OH. DFT calculations, kMC simulations, and experimental studies were combined to reveal the correlation between the structure and selectivity at the atomic level, wherein CoO(111) contributes to CH_4 production and CoO(110) promotes CO formation. We have provided a clear perspective on the reaction mechanism of CoO and found that the C−O bond scission of the $*CH_2O$ intermediate plays a key role in determining CH_4 selectivity. The nature of dissociating C−O bonds was unveiled, which is attributed to the stabilization of *O atoms after C−O bond cleavage and the weakening of C−O bond strength by surface-transferred electrons. These discoveries could give a deep insight into the origin of performance over CoO_x catalysts in CO_2 hydrogenation.

COMPUTATIONAL AND EXPERIMENTAL METHODS

NN-MD Simulations

All calculations with NN-MD were performed by LASP, which is generally applied in large-scale simulation for complex chemical systems via NN potential.[47] The details of the surface reduction-reconstruction method to simulate the reduction process of Co_3O_4 can be found in the Supporting Information.

DFT Calculations

DFT calculations were carried out via Vienna ab initio simulation software.[48,49] The electron exchange and correlation effects were described by the Perdew−Burke−Ernzerhof functional form of the generalized gradient approximation (GGA).[50] In consideration of van der Waals correction for all systems, the DFT-D3 method with Becke−Jonson damping was utilized.[51] The projector augmented wave method was used to describe the interaction between atomic cores and electrons.[52] To solve the Kohn−Sham equations, the plane-wave basis set was employed with a cutoff energy of 400 eV. In addition, the atomic force convergence criterion of force was set to 0.02 eV/Å. For metal oxides, the DFT + U method was applied to better describe the localized 3d electrons of cobalt in CoO, where an effective U value ($U_{eff} = U_{Co} - J_{Co}$ = 3.7 eV) was adopted.[53−55] More details are described in the Supporting Information.

kMC Simulations

Based on the thermodynamic and kinetic parameters calculated by DFT over CoO(111) (Table S1), the kMC method[56] that can simulate the system evolution during the reaction at the molecular level was carried out by software package Zacros[57,58] to simulate the CO_2 hydrogenation reaction. To perform kMC simulations under experimental reaction conditions, the total pressure and the temperature of our reaction system are set to 1 atm and 573 K, respectively. More details are described in the Supporting Information.

Experimental Details

The CoO catalysts were synthesized via a hydrothermal method. To be more specific, 2.4 g of $C_4H_6O_4 \cdot Co \cdot 4H_2O$ and 60 mL of $(CH_2OH)_2$ were added into a three-port round-bottomed flask. The mixture was then heated up to about 433 K. Afterward, 20 mL of 0.5 M K_2CO_3 solution was added. Under constant stirring and a continuous N_2 flow, the slurry was further aged for 0 h and 3 h, respectively. Then, the solid was recovered by centrifugation. We used ultrapurity water and anhydrous ethanol to wash the solid, until the supernatant is neutral (pH = 7). After drying at 343 K overnight, the solid is calcined at 723 K for about 4 h in air. At the moment, as the precursor of CoO, Co_3O_4 catalysts were obtained. Though the further treatment of H_2 at 573 K for 1 h, we finally prepared the CoO catalysts.

The catalytic performance of CoO was tested in a fixed-bed reactor. The reaction condition was set to 573 K and 1 atm. The molar ratio of CO_2 and H_2 was 1:3. In addition, N_2 was the internal standard gas during the reaction. The exhaust streams were analyzed via an online gas chromatograph (GC, Agilent 7890A).

More experimental details are described in the Supporting Information.

ASSOCIATED CONTENT

Supporting Information

The Supporting Information is available free of charge at https://pubs.acs.org/doi/10.1021/jacsau.2c00632.

Experimental details and supporting data (PDF)

AUTHOR INFORMATION

Corresponding Authors

Zhi-Jian Zhao − *Key Laboratory for Green Chemical Technology of Ministry of Education, School of Chemical*

https://doi.org/10.1021/jacsau.2c00632
JACS Au 2023, 3, 508−515

Engineering and Technology, Tianjin University; Collaborative Innovation Center for Chemical Science and Engineering, Tianjin 300072, China; orcid.org/0000-0002-8856-5078; Email: zjzhao@tju.edu.cn

Jinlong Gong − *Key Laboratory for Green Chemical Technology of Ministry of Education, School of Chemical Engineering and Technology, Tianjin University; Collaborative Innovation Center for Chemical Science and Engineering, Tianjin 300072, China; Joint School of National University of Singapore and Tianjin University, International Campus of Tianjin University, Fuzhou 350207, China; Haihe Laboratory of Sustainable Chemical Transformations, Tianjin 300192, China; National Industry-Education Platform of Energy Storage, Tianjin University, Tianjin 300350, China;* orcid.org/0000-0001-7263-318X; Email: jlgong@tju.edu.cn

Authors

Kailang Li − *Key Laboratory for Green Chemical Technology of Ministry of Education, School of Chemical Engineering and Technology, Tianjin University; Collaborative Innovation Center for Chemical Science and Engineering, Tianjin 300072, China*

Xianghong Li − *Key Laboratory for Green Chemical Technology of Ministry of Education, School of Chemical Engineering and Technology, Tianjin University; Collaborative Innovation Center for Chemical Science and Engineering, Tianjin 300072, China*

Lulu Li − *Key Laboratory for Green Chemical Technology of Ministry of Education, School of Chemical Engineering and Technology, Tianjin University; Collaborative Innovation Center for Chemical Science and Engineering, Tianjin 300072, China*

Xin Chang − *Key Laboratory for Green Chemical Technology of Ministry of Education, School of Chemical Engineering and Technology, Tianjin University; Collaborative Innovation Center for Chemical Science and Engineering, Tianjin 300072, China*

Shican Wu − *Key Laboratory for Green Chemical Technology of Ministry of Education, School of Chemical Engineering and Technology, Tianjin University; Collaborative Innovation Center for Chemical Science and Engineering, Tianjin 300072, China*

Chengsheng Yang − *Key Laboratory for Green Chemical Technology of Ministry of Education, School of Chemical Engineering and Technology, Tianjin University; Collaborative Innovation Center for Chemical Science and Engineering, Tianjin 300072, China*

Xiwen Song − *Key Laboratory for Green Chemical Technology of Ministry of Education, School of Chemical Engineering and Technology, Tianjin University; Collaborative Innovation Center for Chemical Science and Engineering, Tianjin 300072, China*

Complete contact information is available at: https://pubs.acs.org/10.1021/jacsau.2c00632

Author Contributions

K.L. performed the theoretical calculation and the experiment. X.L., C.Y., and X.S. contributed to some experimental test and characterization of the catalysts. L.L., X.C., and S.W. contributed to useful discussion. Z.-J.Z. and J.G. designed and directed the project. Z.-J.Z. and J.G. supervised the project. All the authors contributed to the modification of the manuscript. CRediT: **Kailang Li** data curation, formal analysis, investigation, writing-original draft, writing-review & editing; **Xianghong Li** data curation, formal analysis, investigation, methodology, validation, writing-review & editing; **Lulu Li** data curation, formal analysis, investigation, writing-review & editing; **Xin Chang** data curation, formal analysis, investigation, writing-review & editing; **Shican Wu** data curation, formal analysis, investigation, writing-review & editing; **Chengsheng Yang** formal analysis, investigation, methodology; **Xiwen Song** data curation, formal analysis, investigation; **Zhi-Jian Zhao** conceptualization, data curation, formal analysis, funding acquisition, project administration, supervision, validation, writing-original draft, writing-review & editing; **Jinlong Gong** conceptualization, funding acquisition, investigation, project administration, supervision, validation, writing-original draft, writing-review & editing.

Notes

The authors declare no competing financial interest.

■ ACKNOWLEDGMENTS

We acknowledge the National Key R&D Program of China (2021YFA1500704), the National Natural Science Foundation of China (No. 22121004 and U22A20409), the Haihe Laboratory of Sustainable Chemical Transformations, the Program of Introducing Talents of Discipline to Universities (BP0618007), and the XPLORER PRIZE for financial support. We also acknowledge generous computing resources at High Performance Computing Center of Tianjin University.

■ REFERENCES

(1) Jiang, X.; Nie, X.; Guo, X.; Song, C.; Chen, J. G. Recent Advances in Carbon Dioxide Hydrogenation to Methanol via Heterogeneous Catalysis. *Chem. Rev.* **2020**, *120*, 7984−8034.

(2) Zhong, J.; Yang, X.; Wu, Z.; Liang, B.; Huang, Y.; Zhang, T. State of the art and perspectives in heterogeneous catalysis of CO_2 hydrogenation to methanol. *Chem. Soc. Rev.* **2020**, *49*, 1385−1413.

(3) Gao, P.; Zhang, L.; Li, S.; Zhou, Z.; Sun, Y. Novel Heterogeneous Catalysts for CO_2 Hydrogenation to Liquid Fuels. *ACS Cent. Sci.* **2020**, *6*, 1657−1670.

(4) Li, W.; Nie, X.; Jiang, X.; Zhang, A.; Ding, F.; Liu, M.; Liu, Z.; Guo, X.; Song, C. ZrO_2 support imparts superior activity and stability of Co catalysts for CO_2 methanation. *Appl. Catal. B* **2018**, *220*, 397−408.

(5) Li, C.-S.; Melaet, G.; Ralston, W. T.; An, K.; Brooks, C.; Ye, Y.; Liu, Y.-S.; Zhu, J.; Guo, J.; Alayoglu, S.; Somorjai, G. A. High-performance hybrid oxide catalyst of manganese and cobalt for low-pressure methanol synthesis. *Nat. Commun.* **2015**, *6*, 6538.

(6) Xie, C.; Chen, C.; Yu, Y.; Su, J.; Li, Y.; Somorjai, G. A.; Yang, P. Tandem Catalysis for CO_2 Hydrogenation to C_2-C_4 Hydrocarbons. *Nano Lett.* **2017**, *17*, 3798−3802.

(7) Wang, L.; Wang, L.; Zhang, J.; Liu, X.; Wang, H.; Zhang, W.; Yang, Q.; Ma, J.; Dong, X.; Yoo, S. J.; Kim, J.-G.; Meng, X.; Xiao, F.-S. Selective Hydrogenation of CO_2 to Ethanol over Cobalt Catalysts. *Angew. Chem., Int. Ed.* **2018**, *57*, 6104−6108.

(8) He, Z.; Qian, Q.; Ma, J.; Meng, Q.; Zhou, H.; Song, J.; Liu, Z.; Han, B. Water-Enhanced Synthesis of Higher Alcohols from CO_2 Hydrogenation over a Pt/Co_3O_4 Catalyst under Milder Conditions. *Angew. Chem., Int. Ed.* **2016**, *55*, 737−741.

(9) van Etten, M. P. C.; Zijlstra, B.; Hensen, E. J. M.; Filot, I. A. W. Enumerating Active Sites on Metal Nanoparticles: Understanding the Size Dependence of Cobalt Particles for CO Dissociation. *ACS Catal.* **2021**, *11*, 8484−8492.

(10) Parastaev, A.; Muravev, V.; Osta, E. H.; van Hoof, A. J. F.; Kimpel, T. F.; Kosinov, N.; Hensen, E. J. M. Boosting CO_2

hydrogenation via size-dependent metal-support interactions in cobalt/ceria-based catalysts. *Nat. Catal.* **2020**, *3*, 526−533.

(11) Li, W.; Nie, X.; Yang, H.; Wang, X.; Polo-Garzon, F.; Wu, Z.; Zhu, J.; Wang, J.; Liu, Y.; Shi, C.; Song, C.; Guo, X. Crystallographic dependence of CO_2 hydrogenation pathways over HCP-Co and FCC-Co catalysts. *Appl. Catal. B* **2022**, *315*, No. 121529.

(12) Qin, C.; Hou, B.; Wang, J.; Wang, Q.; Wang, G.; Yu, M.; Chen, C.; Jia, L.; Li, D. Crystal-Plane-Dependent Fischer-Tropsch Performance of Cobalt Catalysts. *ACS Catal.* **2018**, *8*, 9447−9455.

(13) Liu, S.; Yang, C.; Zha, S.; Sharapa, D.; Studt, F.; Zhao, Z.-J.; Gong, J. Moderate Surface Segregation Promotes Selective Ethanol Production in CO_2 Hydrogenation Reaction over CoCu Catalysts. *Angew. Chem., Int. Ed.* **2022**, *134*, No. e202109027.

(14) Zijlstra, B.; Broos, R. J. P.; Chen, W.; Oosterbeek, H.; Filot, I. A. W.; Hensen, E. J. M. Coverage Effects in CO Dissociation on Metallic Cobalt Nanoparticles. *ACS Catal.* **2019**, *9*, 7365−7372.

(15) Fan, T.; Liu, H.; Shao, S.; Gong, Y.; Li, G.; Tang, Z. Cobalt Catalysts Enable Selective Hydrogenation of CO_2 toward Diverse Products: Recent Progress and Perspective. *J. Phys. Chem. Lett.* **2021**, *12*, 10486−10496.

(16) Liu, B.; Ouyang, B.; Zhang, Y.; Lv, K.; Li, Q.; Ding, Y.; Li, J. Effects of mesoporous structure and Pt promoter on the activity of Co-based catalysts in low-temperature CO_2 hydrogenation for higher alcohol synthesis. *J. Catal.* **2018**, *366*, 91−97.

(17) Efremova, A.; Rajkumar, T.; Szamosvölgyi, Á.; SÁpi, A.; BaÁn, K.; Szenti, I.; Gómez-Pérez, J.; Varga, G.; Kiss, J.; Halasi, G.; Kukovecz, Á.; Kónya, Z. Complexity of a Co_3O_4 System under Ambient-Pressure CO_2 Methanation: Influence of Bulk and Surface Properties on the Catalytic Performance. *J. Phys. Chem. C* **2021**, *125*, 7130−7141.

(18) Yang, C.; Liu, S.; Wang, Y.; Song, J.; Wang, G.; Wang, S.; Zhao, Z.-J.; Mu, R.; Gong, J. The Interplay between Structure and Product Selectivity of CO_2 Hydrogenation. *Angew. Chem., Int. Ed.* **2019**, *58*, 11242−11247.

(19) Behler, J. Four Generations of High-Dimensional Neural Network Potentials. *Chem. Rev.* **2021**, *121*, 10037−10072.

(20) Zhang, J.; Lei, Y. K.; Zhang, Z.; Chang, J.; Li, M.; Han, X.; Yang, L.; Yang, Y. I.; Gao, Y. Q. A Perspective on Deep Learning for Molecular Modeling and Simulations. *J. Phys. Chem. A* **2020**, *124*, 6745−6763.

(21) Ma, S.; Liu, Z.-P. Machine Learning for Atomic Simulation and Activity Prediction in Heterogeneous Catalysis: Current Status and Future. *ACS Catal.* **2020**, *10*, 13213−13226.

(22) Shi, X.; Lin, X.; Luo, R.; Wu, S.; Li, L.; Zhao, Z.-J.; Gong, J. Dynamics of Heterogeneous Catalytic Processes at Operando Conditions. *JACS Au* **2021**, *1*, 2100−2120.

(23) Cheng, D.; Zhao, Z.-J.; Zhang, G.; Yang, P.; Li, L.; Gao, H.; Liu, S.; Chang, X.; Chen, S.; Wang, T.; Ozin, G. A.; Liu, Z.-P.; Gong, J. The nature of active sites for carbon dioxide electroreduction over oxide-derived copper catalysts. *Nat. Commun.* **2021**, *12*, 395.

(24) ten Have, I. C.; Kromwijk, J. J. G.; Monai, M.; Ferri, D.; Sterk, E. B.; Meirer, F.; Weckhuysen, B. M. Uncovering the reaction mechanism behind CoO as active phase for CO_2 hydrogenation. *Nat. Commun.* **2022**, *13*, 324.

(25) Wang, M.; Zhang, G.; Zhu, J.; Lia, W.; Wang, J.; Bian, K.; Liu, Y.; Ding, F.; Song, C.; Guo, X. Unraveling the Tunable Selectivity on Cobalt Oxide and Metallic Cobalt Sites for CO_2 Hydrogenation. *Chem. Eng. J.* **2022**, *446*, No. 137217.

(26) Ko, J.; Kim, B. K.; Han, J. W. Density Functional Theory Study for Catalytic Activation and Dissociation of CO_2 on Bimetallic Alloy Surfaces. *J. Phys. Chem. C* **2016**, *120*, 3438−3447.

(27) Xu, D.; Wang, Y.; Ding, M.; Hong, X.; Liu, G.; Tsang, S. C. E. Advances in Higher Alcohol Synthesis from CO_2 Hydrogenation. *Chem* **2021**, *7*, 849−881.

(28) Chen, C.; Wang, Q.; Wang, G.; Hou, B.; Jia, L.; Li, D. Mechanistic Insight into the C_2 Hydrocarbons Formation from Syngas on fcc-Co(111) Surface: A DFT Study. *J. Phys. Chem. C* **2016**, *120*, 9132−9147.

(29) Banerjee, A.; van Bavel, A. P.; Kuipers, H. P. C. E.; Saeys, M. CO Activation on Realistic Cobalt Surfaces: Kinetic Role of Hydrogen. *ACS Catal.* **2017**, *7*, 5289−5293.

(30) Kattel, S.; Liu, P.; Chen, J. G. Tuning Selectivity of CO_2 Hydrogenation Reactions at the Metal/Oxide Interface. *J. Am. Chem. Soc.* **2017**, *139*, 9739−9754.

(31) Vogt, C.; Monai, M.; Kramer, G. J.; Weckhuysen, B. M. The renaissance of the Sabatier reaction and its applications on Earth and in space. *Nat. Catal.* **2019**, *2*, 188−197.

(32) Ye, R.-P.; Ding, J.; Gong, W.; Argyle, M. D.; Zhong, Q.; Wang, Y.; Russell, C. K.; Xu, Z.; Russell, A. G.; Li, Q.; Fan, M.; Yao, Y.-G. CO_2 hydrogenation to high-value products via heterogeneous catalysis. *Nat. Commun.* **2019**, *10*, 5698.

(33) Roy, S.; Cherevotan, A.; Peter, S. C. Thermochemical CO_2 Hydrogenation to Single Carbon Products: Scientific and Technological Challenges. *ACS Energy Lett.* **2018**, *3*, 1938−1966.

(34) Ocampo-Restrepo, V. K.; Verga, L. G.; Da Silva, J. L. F. Ab Initio Study of the C-O Bond Dissociation in CO_2 Reduction by Redox and Carboxyl Routes on 3d Transition Metal Systems. *J. Phys. Chem. C* **2021**, *125*, 26296−26306.

(35) Stegelmann, C.; Andreasen, A.; Campbell, C. T. Degree of Rate Control: How Much the Energies of Intermediates and Transition States Control Rates. *J. Am. Chem. Soc.* **2009**, *131*, 8077−8082.

(36) Xie, X.; Li, Y.; Liu, Z.-Q.; Haruta, M.; Shen, W. Low-temperature oxidation of CO catalysed by Co_3O_4 nanorods. *Nature* **2009**, *458*, 746−749.

(37) Liotta, L. F.; Carlo, G. D.; Pantaleo, G.; Venezia, A. M.; Deganello, G. Co_3O_4/CeO_2 composite oxides for methane emissions abatement: Relationship between Co_3O_4-CeO_2 interaction and catalytic activity. *Appl. Catal. B* **2006**, *66*, 217−227.

(38) Biesinger, M. C.; Payne, B. P.; Grosvenor, A. P.; Lau, L. W. M.; Gerson, A. R.; Smart, R. S. Resolving surface chemical states in XPS analysis of first row transition metals, oxides and hydroxides: Cr, Mn, Fe, Co and Ni. *Appl. Surf. Sci.* **2011**, *257*, 2717−2730.

(39) Chen, Z.; Kronawitter, C. X.; Koel, B. E. Facet-dependent activity and stability of Co_3O_4 nanocrystals towards the oxygen evolution reaction. *Phys. Chem. Chem. Phys.* **2015**, *17*, 29387−29393.

(40) Wu, C.; Lin, L.; Liu, J.; Zhang, J.; Zhang, F.; Zhou, T.; Rui, N.; Yao, S.; Deng, Y.; Yang, F.; Xu, W.; Luo, J.; Zhao, Y.; Yan, B.; Wen, X.-D.; Rodriguez, J. A.; Ma, D. Inverse ZrO_2/Cu as a highly efficient methanol synthesis catalyst from CO_2 hydrogenation. *Nat. Commun.* **2020**, *11*, 5767.

(41) Wang, Y.; Kattel, S.; Gao, W.; Li, K.; Liu, P.; Chen, J. G.; Wang, H. Exploring the ternary interactions in Cu-ZnO-ZrO_2 catalysts for efficient CO_2 hydrogenation to methanol. *Nat. Commun.* **2019**, *10*, 1166.

(42) Kelly, T. G.; Stottlemyer, A. L.; Ren, H.; Chen, J. G. Comparison of O−H, C−H, and C−O Bond Scission Sequence of Methanol on Tungsten Carbide Surfaces Modified by Ni, Rh, and Au. *J. Phys. Chem. C* **2011**, *115*, 6644−6650.

(43) Kattel, S.; Yu, W.; Yang, X.; Yan, B.; Huang, Y.; Wan, W.; Liu, P.; Chen, J. G. CO_2 Hydrogenation over Oxide-Supported PtCo Catalysts: The Role of the Oxide Support in Determining the Product Selectivity. *Angew. Chem., Int. Ed.* **2016**, *55*, 7968−7973.

(44) Zheng, Y.; Li, K.; Wang, H.; Wang, Y.; Tian, D.; Wei, Y.; Zhu, X.; Zeng, C.; Luo, Y. Structure dependence and reaction mechanism of CO oxidation: A model study on macroporous CeO_2 and CeO_2-ZrO_2 catalysts. *J. Catal.* **2016**, *344*, 365−377.

(45) Konsolakis, M.; Ioakimidis, Z.; Kraia, T.; Marnellos, G. E. Hydrogen Production by Ethanol Steam Reforming (ESR) over CeO_2 Supported Transition Metal (Fe, Co, Ni, Cu) Catalysts: Insight into the Structure-Activity Relationship. *Catalysts* **2016**, *6*, 39.

(46) Pawlak, D. A.; Ito, M.; Oku, M.; Shimamura, K.; Fukuda, T. Interpretation of XPS O (1s) in Mixed Oxides Proved on Mixed Perovskite Crystals. *J. Phys. Chem. B* **2002**, *106*, 504−507.

(47) Huang, S.-D.; Shang, C.; Kang, P. L.; Zhang, X.-J.; Liu, Z.-P. Material discovery by combining stochastic surface walking global optimization with a neural network. *Chem. Sci.* **2017**, *8*, 6327−6337.

(48) Kresse, G.; Furthmüller, J. Efficiency of ab-initio total energy calculations for metals and semiconductors using a plane-wave basis set. *Comp. Mater. Sci.* **1996**, *6*, 15−50.

(49) Kresse, G.; Hafner, J. Ab initio molecular-dynamics simulation of the liquid-metal-amorphous-semiconductor transition in germanium. *Phys. Rev. B* **1994**, *49*, 14251−14269.

(50) Perdew, J. P.; Burke, K.; Ernzerhof, M. Generalized Gradient Approximation Made Simple. *Phys. Rev. Lett.* **1996**, *77*, 3865−3868.

(51) Grimme, S.; Ehrlich, S.; Goerigk, L. Effect of the damping function in dispersion corrected density functional theory. *J. Comput. Chem.* **2011**, *32*, 1456−1465.

(52) Kresse, G.; Joubert, D. From ultrasoft pseudopotentials to the projector augmented-wave method. *Phys. Rev. B* **1999**, *59*, 1758−1775.

(53) Kulika, H. J.; Marzari, N. Systematic study of first-row transition-metal diatomic molecules: A self-consistent DFT+U approach. *J. Chem. Phys.* **2010**, *133*, 114103.

(54) Youmbi, B. S.; Calvayrac, F. Structure of CoO(001) surface from DFT + U calculations. *Surf. Sci.* **2014**, *621*, 1−6.

(55) Wang, L.; Maxisch, T.; Ceder, G. Oxidation energies of transition metal oxides within the GGA+U Framework. *Phys. Rev. B* **2006**, *73*, No. 195107.

(56) Andersen, M.; Panosetti, C.; Reuter, K. A Practical Guide to Surface Kinetic Monte Carlo Simulations. *Front. Chem.* **2019**, *7*, 202.

(57) Stamatakis, M.; Vlachos, D. G. Unraveling the Complexity of Catalytic Reactions via Kinetic Monte Carlo Simulation: Current Status and Frontiers. *ACS Catal.* **2012**, *2*, 2648−2663.

(58) Stamatakis, M.; Vlachos, D. G. A graph-theoretical kinetic Monte Carlo framework for on-lattice chemical kinetics. *J. Chem. Phys.* **2011**, *134*, 214115.

https://doi.org/10.1021/jacsau.2c00632
JACS Au 2023, 3, 508−515